

©2020, Elsevier. Licensed under the Creative Commons Attribution-NonCommercial-NoDerivatives 4.0 International <http://creativecommons.org/about/downloads>



A comparative analysis of shielding of thermal radiation of fires using mist curtains containing droplets of pure water or sea water

Leonid A. Dombrovsky^{a,b,c,1}, Vladimir Yu. Levashov^d, Alexei P. Kryukov^e,
Siaka Dembele^a, and Jennifer X. Wen^f

^aDepartment of Mechanical Engineering, Kingston University, London, SW15 3DW, UK

^bJoint Institute for High Temperatures, 17A Krasnokazarmennaya St, Moscow, 111116, Russia

^cThe University of Tyumen, 6 Vолодарский St, Tyumen, 625003, Russia

^dInstitute of Mechanics of Moscow State University, 1 Michurinskiy Prospekt, Moscow, 119192, Russia

^eMoscow Power Engineering Institute, 14 Krasnokazarmennaya St, Moscow, 111250, Russia

^fSchool of Engineering, University of Warwick, Coventry CV4 7AL, UK

Abstract

The paper is focused on comparative computational modelling of the attenuation of fire radiation by water mists of pure water or sea water. The use of sea water in fire protection could be a more convenient and practical choice in coastal areas, on offshore installations or transported ships. The spectral absorption and scattering properties of both water droplets and salt particles formed by evaporation of sea water droplets are considered. A combined heat transfer problem is based on a combination of the spectral radiative transfer in a mist curtain, the kinetics of water evaporation, and convective heat transfer along the curtain. The developed computational model is used to analyze the radiative heating and evaporation of droplets of pure water and more complex multi-phase processes in droplets of sea water at all stages of the process. The numerical results for the case problem indicate sufficiently good shielding quality of a sea-water mist curtain. The suggested approach is expected to be useful for important engineering applications in fire protection.

Keywords: Fire radiation; Water mist; Sea water droplets; Radiative heat transfer; Evaporation.

¹ Corresponding author. Tel. +7 910 408 0186
Email address: ldombr@yandex.ru

Nomenclature

a	radius of droplet or particle	μ	cosine of an angle
c	specific heat capacity	ρ	density
C	coefficient introduced by Eq. (1b)	$\bar{\rho}$	coefficient introduced by Eq. (1b)
C_D	drag coefficient	σ	scattering coefficient
d	thickness of mist curtain	σ_0	Stefan–Boltzmann constant
D	diffusion coefficient	τ	optical thickness
E	normalized absorption or scattering coefficient	φ	air humidity
f_v	volume fraction of particles	ψ	coefficient introduced by Eq. (16)
f_{ev}	coefficient in Eq. (18)	χ	coefficient introduced by Eq. (1b)
g	acceleration of gravity	ω	albedo of single scattering
G	irradiation		
H	height of the mist curtain		
I	intensity of radiation		
J^\pm	hemispherical components of radiation intensity		
k	thermal conductivity		
L	latent heat of evaporation		
\dot{m}	mass flow rate of evaporation		
M	molecular weight		
n	index of refraction		
Nu	Nusselt number		
p	pressure of gas		
Pr	Prandtl number		
q	radiative flux		
Q	efficiency factor of absorption or scattering		
R	gas constant		
\bar{R}	coefficient introduced by Eq. (6)		
Re	Reynolds number		
s	salinity		
t	time		
T	temperature		
u	velocity		
W	absorbed radiation power		
x	diffraction (size) parameter		
y	horizontal coordinate		
z	vertical coordinate		

Greek symbols

α	absorption coefficient
β	extinction coefficient
γ	coefficient in Eq. (13b)
δ	wall thickness of hollow particle
ε	emissivity
ζ	exponent introduced by Eq. (2)
η	dynamic viscosity
κ	index of absorption
λ	wavelength

Subscripts and superscripts

a	absorption
air	air
b	blackbody
d	droplet
e	external
ev	evaporation
f	flame
K	Knudsen
max	maximum
rad	radiation
rel	relaxation
rem	remaining
R	Rayleigh
s	scattering
salt	salt
sat	saturation
sw	sea water
tr	transport
w	water
λ	spectral
0	initial

1. Introduction

Water mist curtains have received considerable attention from researchers and engineers for protection against thermal radiation from fires, as reviewed in reference [1]. In the past two decades, there has been significant progress in the physical analysis and computational modelling of combined heat transfer processes in sprays for fire protection. A detailed description of radiative transfer in computational studies of water mists is combined in some papers with studies of heat, mass and momentum transfer in sprays taking into account both dynamic and thermal non-equilibrium of droplets and ambient gas [2–9].

As one can expect, the complexity of general computational models is an obstacle to their widespread use. The relatively simple engineering approach suggested in [10, 11] is considered by the authors as a good alternative basis for engineering applications. A series of calculations enabled us to suggest a decrease in the size of supplied water droplets with the distance from the irradiated side of the mist layer to improve the shielding properties of the mist curtain. At the same time, it is clear now that the model of evaporation of water droplets used in [10, 11] is too simplified and should be improved. The vast majority of the literature studies on water sprays in fire protection are concerned with pure water, for which the optical properties could be easily obtained for the calculations of the radiative properties of droplets. The use of different chemical additives to enhance the fire suppression potential was investigated in few studies [12]. The scope of the present paper is fire radiation shielding by water sprays/mist curtains, and not fire suppression where the water is sprayed directly onto the flame. In the water spray/mist curtain application, the intention is to provide some shielding protection between the source of the fire and potential targets (e.g. humans, flammable targets). The study of water sprays made of water with additives or impure salt sea water in fire radiation shielding is an area of research scarce in the literature.

Although pure water is the natural choice in water spray/mist fire applications, the use of impure, salty sea water could be a practical and more convenient solution in some cases where pure water is not available. These include for example coastal areas, offshore platforms or human/goods maritime transportation ships where sea water could be a good alternative to be used as spray for fire protection applications. The motivation of the current study is to provide a better insight and understanding into the fire radiation shielding of salty sea water sprays and its comparison to the conventional pure water sprays. It is worth noting that, although the optical and thermal properties of sea water are similar to those of pure water, the evaporation of sea water droplets increases the salinity of water droplets and lead to formation of dry particles of sea salt. As a result, both the optical and thermal properties of particles formed in some sections

of a sea-water curtain are different from the properties of partially evaporated water droplets. This important difference also motivates the current study.

To the best of the authors knowledge, the current literature does not contain studies for the experimental or computational analysis of sea water in fire radiation shielding. The present work is focused on modelling the complex behaviour of sea water droplets during their evaporation and subsequent solidification under the action of intense flame radiation. The process of evaporation of these droplets including formation of solid crust on the droplet surface and subsequent appearance of both hollow thin-walled particles and numerous small crystals of salt makes the problem much more complicated than the case for pure water. Moreover, one cannot ignore specific infrared optical properties of salt particles which should be accounted for. The computational model and computer code for such a composite curtain should be significantly modified as well.

In contrast to [10, 11] we do not consider the variants of variable parameters of supplied water droplets in the initial cross section of the mist curtain. This technical complication of the problem statement seems to be not reasonable at the present stage of our study. As before (and in many other papers), the isothermal droplets are considered by neglecting the relatively small effect of a nonuniform absorption of radiation by asymmetrically irradiated droplets [13]. A considerably better approach for kinetics of evaporation is employed in the present paper.

The main objective of the present paper is two-fold: (1) to develop a simple but complete model for coupled heat transfer processes in a semi-transparent layer of evaporating sea water droplets considered as a shield for infrared radiation of fires, (2) to compare computationally the shielding properties of water mists containing pure and sea water droplets.

The model suggested in the paper is relatively simple because it is based on several assumptions. These assumptions are physically sound but lead to systematic errors in calculations of the radiation shielding for real mist curtains. Fortunately, we are focused mainly on a comparative analysis of mist curtains containing droplets of pure water or sea water. It is expected that the mentioned systematic errors do not effect on the qualitative results of the comparative computational study.

2. Spectral properties of mist curtain particles

2.1. Optical constants of pure and sea water and optical properties of water droplets

The spectral optical constants of pure water are well known [14]. For convenience of subsequent analysis, spectral dependences of these quantities in the most important part of the infrared range are presented in Fig. 1. According to paper [15], the comparison of optical constants of standard sea water (SSW) [16] at room temperature and those for pure water show

that the effect of salinity of $s = 3.5\%$ on both index of refraction, n_w , and index of absorption, κ_w , in the most important wavelength range of $1 < \lambda < 6 \mu\text{m}$ is very small. In addition to [15], one can refer to recent data of [17] for optical constants of sodium chloride solution at room temperature in the wavelength range of $0.3 < \lambda < 2.5 \mu\text{m}$. The spectral dependences plotted in Fig. 2 confirm that near-infrared properties of saline water, which is similar to sea water, are almost the same as those of pure water.

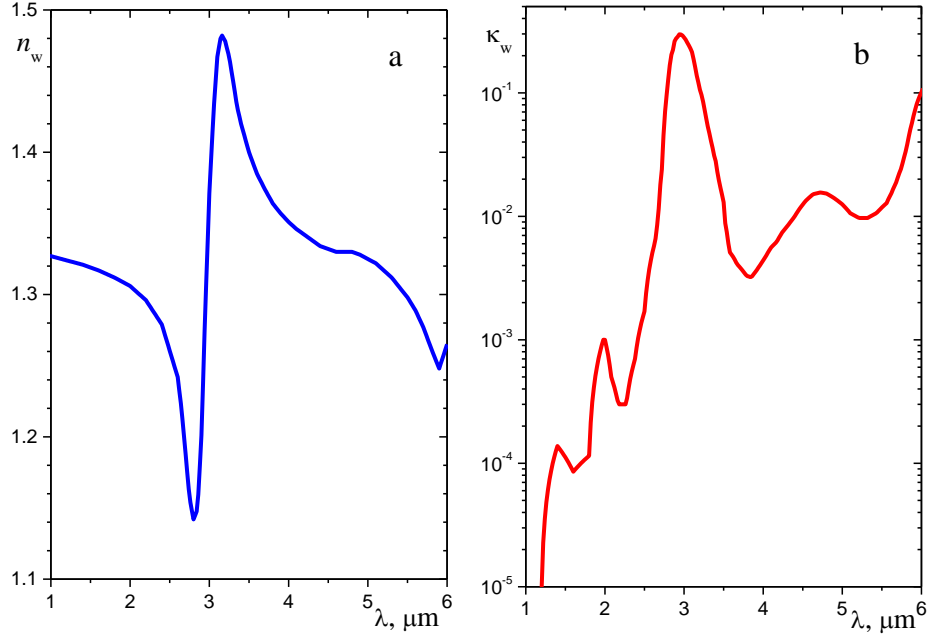


Fig. 1. Spectral indices of (a) refraction and (b) absorption of pure water.

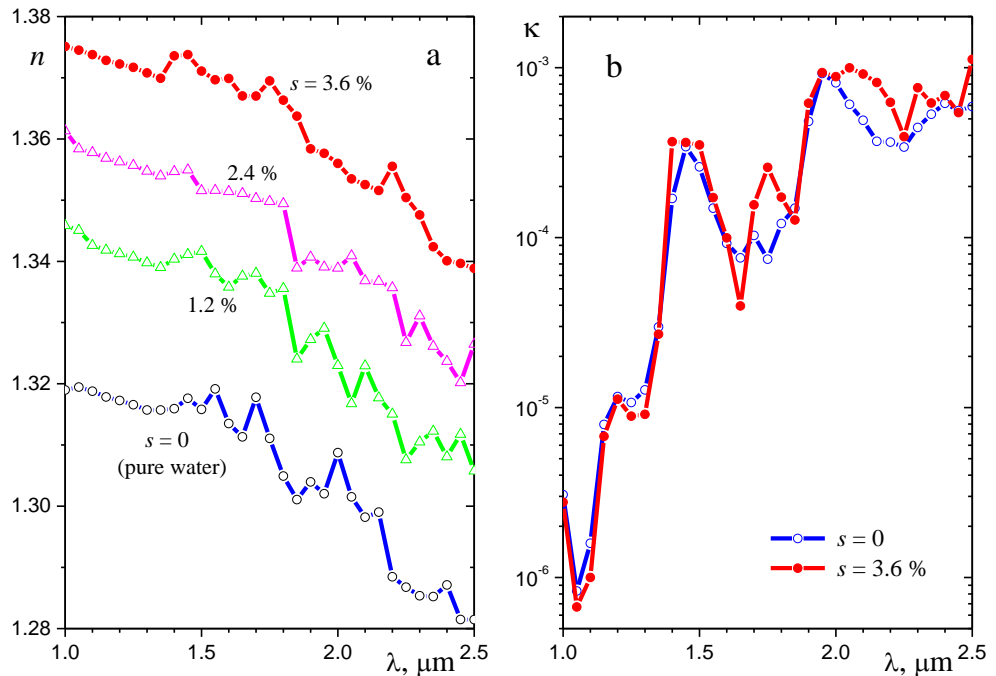


Fig. 2. Spectral indices of (a) refraction and (b) absorption of NaCl solution [16].

According to [10], the average Sauter radius of supplied water droplets is in the range of $30 < a_{32} < 100 \mu\text{m}$. Note that the monodisperse approximation, where all the droplets in a local volume are assumed to have the same Sauter radius, is applicable to the problem under consideration [18, 19]. The diffraction parameter of these droplets, $x = 2\pi a_{32}/\lambda$, which is also called the size parameter, determines the regime of absorption and scattering of radiation by the droplet. The rigorous Mie theory is true for water droplets at arbitrary values of x . However, the spectral calculations of absorption and scattering properties of water droplets with the use of Mie theory are usually time-consuming, especially for large droplets. Fortunately, the general solution degenerates in two limiting ranges of diffraction parameter. For small water droplets as compared with the radiation wavelength (at $x \ll 1$), it is sufficient to consider the dipole scattering. This is the so-called Rayleigh regime, characterized by a predominant absorption and insignificant scattering. In the opposite case of optically large droplets ($x \gg 1$) typical for water droplets at the initial cross section of the mist curtain, when $x > 30$, the geometrical optics (GO) approximation can be used instead of the Mie theory to calculate the main absorption and scattering characteristics of these droplets: the efficiency factor of absorption, Q_a , and the transport efficiency factor of scattering, Q_s^{tr} [19]. In the case of large particles, the latter value decreases with the diffraction parameter because of predominant forward scattering. So, the transport efficiency factor of scattering for water droplets appears to be small for both small and very large droplets (as compared with the radiation wavelength). As a result, the most significant scattering effects are observed at intermediate values of x . This is the so-called Mie scattering region [19]. It will be shown below that the effect of strong Mie scattering takes place for partially evaporated water droplets of the mist curtain.

There are three dimensionless characteristics which determine the optical properties of droplets in the GO limit: the indices of refraction and absorption and the optical thickness of the droplet, $\tau = 4\kappa x$. In the case of optically thin droplets ($\tau \ll 1$), one can use the exact analytical solution derived in [20] as it was done for ice grains in [21]. However, the optical thickness of water droplets is large in the spectral absorption band of water. Therefore, following [10], we will use the approximate expressions suggested in [22] for semi-transparent particles (see also [19]):

$$Q_a = \frac{4n}{(n+1)^2} [1 - \exp(-\tau)] \quad Q_s^{\text{tr}} = C \begin{cases} \bar{\rho}/5 & \text{when } \bar{\rho} \leq 5 \\ (5/\bar{\rho})^\chi & \text{when } \bar{\rho} > 5 \end{cases} \quad (1a)$$

where

$$C = 1.5n(n-1)\exp(-15\kappa) \quad \bar{\rho} = 2x(n-1) \quad \chi = 1.4 - \exp(-80\kappa) \quad (1b)$$

Equations (1a)–(1b) can be used at arbitrary values of x , including the Mie scattering region, not only in the GO limit. This is important because the size of droplets decreases during their evaporation. The error of the above approximation is insignificant in the spectral range under consideration. This is illustrated for droplets of pure water in Fig. 3, where the most important spectral values of Q_a and transport albedo of single scattering, $\omega_{tr} = Q_s^{\text{tr}} / (Q_a + Q_s^{\text{tr}})$, are presented.

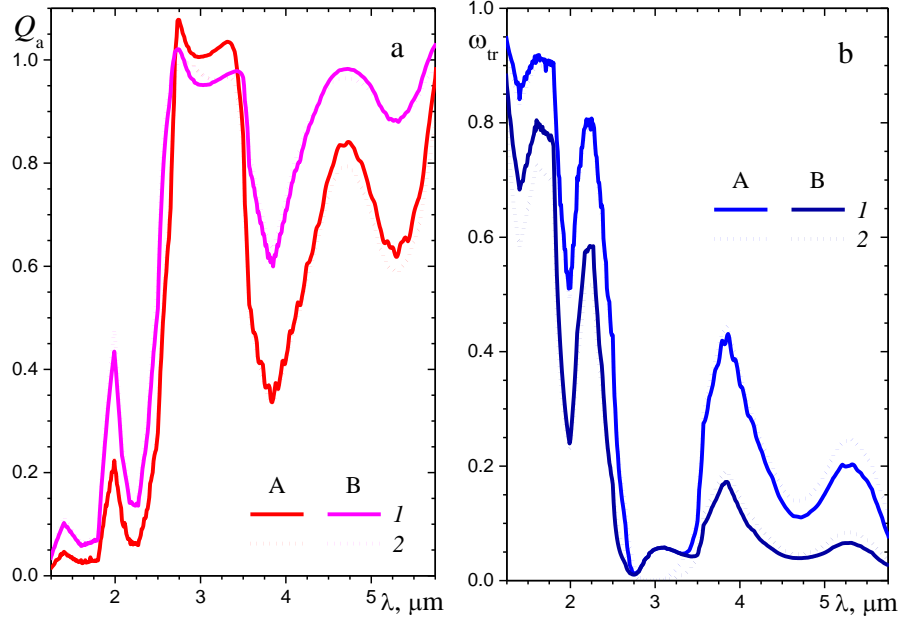


Fig. 3. Spectral dependences of (a) absorption efficiency factor and (b) transport albedo of single scattering for droplets of pure water: A – $a = 20 \mu\text{m}$, B – $a = 50 \mu\text{m}$; I – exact Mie solution, 2 – approximation (1a,b).

2.2. Optical constants of sea salt and concentrated sea water

There are only few publications on infrared optical constants of sea salt and also on optical constants of sodium chloride which is the main component of sea salt. The average constant value of $n_{\text{salt}} = 1.45$ was recommended in early paper by Volz [23] for the wavelength range of $2.5 \leq \lambda < 6 \mu\text{m}$. However, more accurate spectral dependence $n_{\text{salt}}(\lambda)$ suggested by Shettle and Fenn [24] for wider wavelength range (see Fig. 4a) is used in subsequent calculations. The infrared spectral data for $\kappa_{\text{salt}}(\lambda)$ reported in paper [23] were also extended in [24] up to the wavelength of $\lambda = 0.2 \mu\text{m}$. So, we use the interpolated data of [24] at $\lambda < 2.5 \mu\text{m}$:

$$\kappa_{\text{salt}} = 10^\zeta \quad \zeta = \begin{cases} -11.5\lambda - 2.25 & \text{when } 0.3 \leq \lambda < 0.5 \mu\text{m} \\ 7.2\lambda - 11.6 & \text{when } 0.5 \leq \lambda < 1.1 \mu\text{m} \\ 0.97\lambda - 4.46 & \text{when } 1.1 \leq \lambda < 2.5 \mu\text{m} \end{cases} \quad (2)$$

At the same time, more detailed data of [23] are used in the wavelength range of $2.5 \leq \lambda < 6 \mu\text{m}$ (see Fig. 4b). It should be noted that the index of absorption of sea salt is significantly less than that of pure water in the wavelength range of $\lambda > 2.8 \mu\text{m}$ (compare Figs. 1b and 4b).

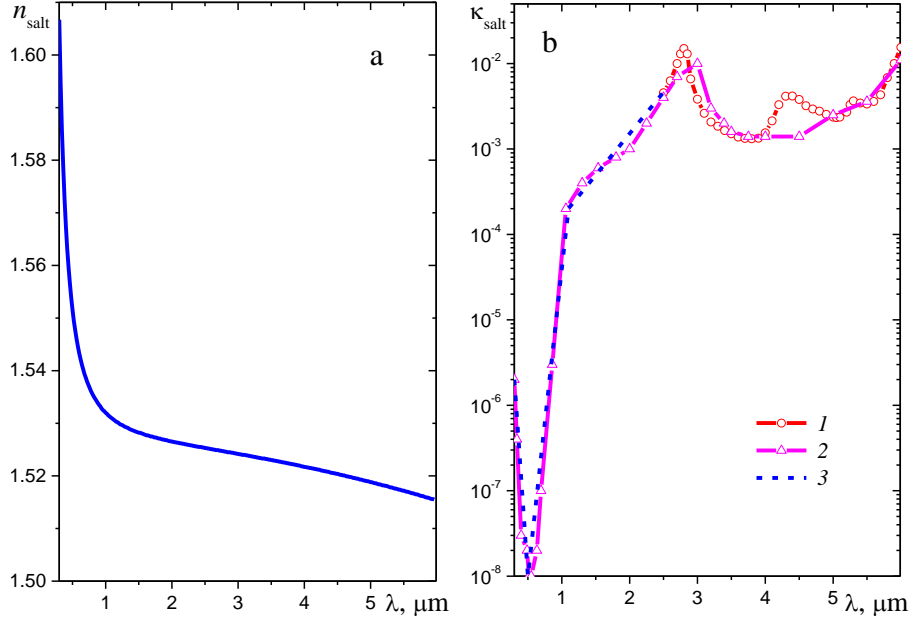


Fig. 4. Infrared indices of (a) refraction and (b) absorption of sea salt:
1 – data reported in [23], 2 – data reported in [24], 3 – interpolation (2).

As one can expect, the optical constants of sea water are intermediate between those of pure water and dry sea salt. However, it was found by Irshad et al. [25] that the volume mixing rule recommended in [24] and employed in [26] provide inaccurate results for sea water compared to direct measurements. This was explained in [25] by dissociation of salt ions upon dissolution of the salt. The latter means that the resulting solution cannot merely be considered as a mixture of whole salt particles and water.

It is difficult to obtain the dependence of optical constants on salinity of partially evaporated sea water using the graphs of paper [25]. However, one can use experimental data of [17] for optical constants of sodium chloride solution at room temperature for qualitative estimates. One can see in Fig. 2a that index of refraction increases almost linearly with salinity of water in the range of $0 < s < 3.6\%$. It should be recalled that solubility of sodium chloride in water is weakly sensitive to water temperature and it is about $s_{\max} = 40\%$ in hot water [27, 28]. The formal linear extrapolation of the dependence of $n_{sw}(s)$ gives too large values of $n_{sw} = 1.9 - 2.0$ at $s = s_{\max}$ in the wavelength range of $1 < \lambda < 2.5 \mu\text{m}$, whereas the index of refraction of dry sodium chloride varies from $n_{salt} = 1.532$ to 1.525 in the same spectral range (see Fig. 4). It means that the effect of salinity on refraction of saline water is not linear over the whole range of s .

We use the following simple approximations for spectral indices of refraction and absorption of sea water in our computational estimates:

$$n_{sw}(\lambda) = n_w - (n_{salt} - n_w) s^{0.5} \quad \kappa_{sw}(\lambda) = \kappa_w - (\kappa_{salt} - \kappa_w) s \quad (3)$$

where $n_{\text{salt}}(\lambda)$ is the spectral dependence recommended in [24] for sea salt, $\kappa_{\text{salt}}(\lambda)$ is the combined analytical approximation (2) and approximation of the data reported in [23] (see curves 3 and 1 in Fig. 4), $n_w(\lambda)$ and $\kappa_w(\lambda)$ are the known functions for pure water. It is expected that the above approximations for optical constants of sea salt and concentrated (partially evaporated) sea water will enable us to obtain qualitatively true computational results on the shielding effect of a mist curtain with the use of sea water instead of pure water.

2.3. Optical properties of saline water droplets and salt particles

It is assumed that the first stage of evaporation of sea water droplets in a mist curtain is finished at the salinity of $s = s_{\text{max}} = 40\%$. In the case of 100 μm initial radius of the droplets, it means that the minimum radius of these droplets before the beginning of solidification is equal to $a \approx 50.6 \mu\text{m}$. After this first stage of the process, the solid crust of sea salt is formed at the droplet surface [29]. Most likely, the increasing pressure of water vapor inside such a composite particle will lead to a local destruction of the crust and the remaining water will be removed from the particle. The photographs of the produced hollow salt particles were given in paper [29]. Similar images of numerous protein particles with orifices can be found in recent paper [30]. The book chapter by Fairhurst [31] containing interesting illustrations from the early paper [32] should be mentioned as well. According to [32], the process just after the first crystals forming is so fast that “the crust did not have time to completely cover the droplet. As the crust neared completion, the liquid was drawn away from the open area leaving a sizable crater in the crust. When fractured and viewed under the microscope, the dried particle proved to be a very thin shell composed of large crystals”. It is also interesting to remind the formation of hollow bubble-like solid particles in nuclear melt-coolant interaction [33].

In the simplified model of the present paper, we will skip the relatively fast process started from the beginning of the salt crust formation on the surface of sea water droplet and finished by formation of almost spherical hollow particle of dry salt. This makes it interesting to compare the spectral optical properties of a sea water droplet of the s_{max} salinity and the optical properties of a hollow salt particle of the same size. The maximum wall thickness of the salt particle, δ_{max} , can be obtained assuming that there is no salt in water surrounded by the salt crust of the droplet. In this case, the mass balance of salt leads to the following estimate:

$$\delta_{\text{max}} = a \left(1 - \sqrt[3]{1 - s_{\text{max}}} \right) = 7.92 \mu\text{m} \quad (4)$$

One can also imagine the situation when water removed from the central part of the particle covered by the salt crust is not pure but it is characterized by the remaining salinity $s_{\text{rem}} < s_{\text{max}}$.

In this case, numerous small particles of sea salt will be formed from this water and the wall thickness of the “mother” particle is determined as follows:

$$\delta = a \left(1 - \sqrt[3]{\frac{1 - s_{\max}}{1 - s_{\text{rem}}}} \right) \quad (5)$$

Assuming that $s_{\text{rem}} = s_{\max}/2$, we obtain $\delta = 4.63 \mu\text{m}$. Most likely, the optical properties of small salt particles formed from the spray of salt water during the hollow particle formation can be calculated using the Rayleigh theory. This is the case when a typical radius of these salt particles, a_s , is about $1 \mu\text{m}$ or less. Small salt particles do not scatter the radiation and absorption coefficient of a cloud of Rayleigh particles does not depend on the particle size. The specific absorption coefficient (per unit volume fraction of particles) is as follows [19]:

$$E_{a,R} = 1.5\pi \frac{\bar{R}}{\lambda} \quad \bar{R} = \frac{24n_{\text{salt}}\kappa_{\text{salt}}}{(n_{\text{salt}}^2 - \kappa_{\text{salt}}^2 + 2)^2 + 4n_{\text{salt}}^2\kappa_{\text{salt}}^2} \quad (6)$$

Equation (6) is true for the spherical particles only. However, according to [34], we will use this solution in estimates for the real cubic salt crystals.

The values of E_a and E_s^{tr} for hollow salt particles can be calculated using the generalized Mie theory for two-layered concentric spheres [19]. The results of these calculations are presented in Fig. 5. One can see that there is a strong maximum of absorption at the wavelength $\lambda = 2.8 \mu\text{m}$ and the value of E_a increases monotonically with the wall thickness δ over the whole spectrum. On the contrary, the scattering has a minimum at $\lambda = 2.8 \mu\text{m}$, whereas the effect of δ on E_s^{tr} is insignificant.

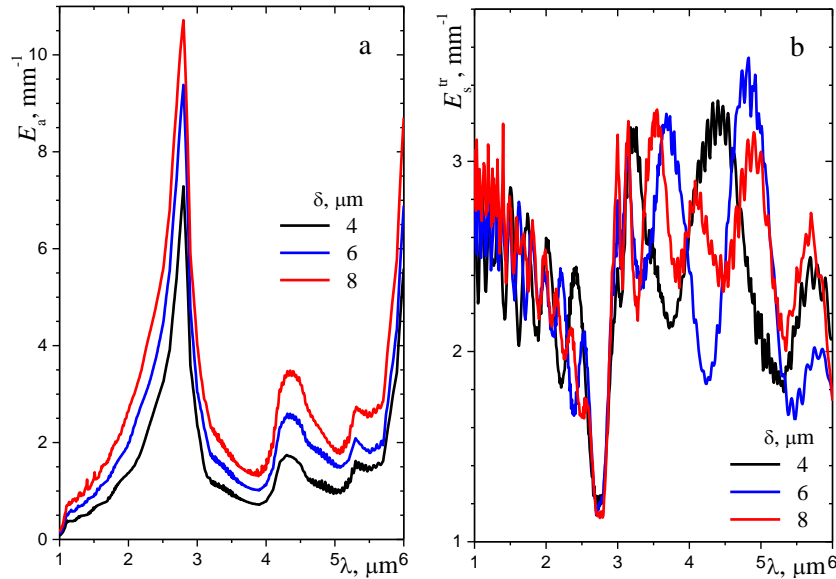


Fig. 5. Normalized coefficients of (a) absorption and (b) transport scattering for hollow spherical particles of sea salt.

Both the hollow particles and small Rayleigh particles of salt can be taken into account using the normalized total absorption coefficient (per unit volume fraction of hollow particles):

$$\bar{E}_a = E_a + E_{a,R} s_{\text{rem}} (1 - s_{\text{max}}) / (1 - s_{\text{rem}}) \quad (7)$$

The calculations showed that the spectral dependences of absorption at different values of the remaining salinity are similar to each other (see Fig. 6). A contribution of small salt particles to the total absorption of infrared radiation is significant only in the narrow wavelength region in the vicinity of the peak of absorption.

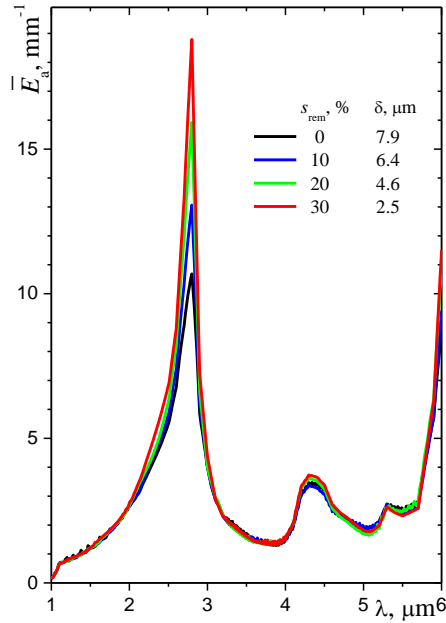


Fig. 6. Normalized total coefficient of absorption for the composite cloud containing hollow particles with radius $a = 50.6 \mu\text{m}$ and small spherical particles of sea salt.

The result obtained indicates that the growing rate of salt crust on the surface of a solidified droplet of sea water is also a parameter of the problem. Strictly speaking, the characteristic time of the impermeable crust formation should be compared with the time of a significant increase in vapor pressure inside the particle. The crust is destroyed when the tensile stress in the crust exceeds the ultimate tensile stress in a polycrystalline sea salt. It should be recalled that similar theoretical estimates have been performed in papers [33, 35, 36] as applied to solidified particles of core melt in the case of a hypothetic severe accident of nuclear reactor. For simplicity, we neglect the time of solid crust formation in the present paper.

3. Radiative transfer model

To choose a relatively simple but physically sound model for transfer of a flame radiation through water mist curtains, consider the main characteristics of the real problem. First of all, the optical thickness of the mist layer should not be too small to reach a significant attenuation

of the incident flame radiation. Therefore, the problem under consideration is characterized by multiple scattering at least in the range of water semi-transparency where the scattering cannot be neglected. In the case of multiple scattering, the details of scattering phase function are not important and one can use the simplest transport approximation [19, 37].

Following the method of [10, 38], a set of 1-D problems for several horizontal layers of the mist curtain (along the layers 1...N in Fig. 7) is used instead of more complicated 2-D radiative transfer problem. The schematic presentation of the problem in Fig. 7 makes also clear the other assumptions of the computational model: (1) The mist of water droplets is generated by a set of small nozzles at the top of the mist layer; (2) The flat mist layer of constant thickness is considered in the model; (3) One side of the mist layer is diffusely irradiated by the flame which is also flat but a variation of radiative flux with the height can be taken into account.

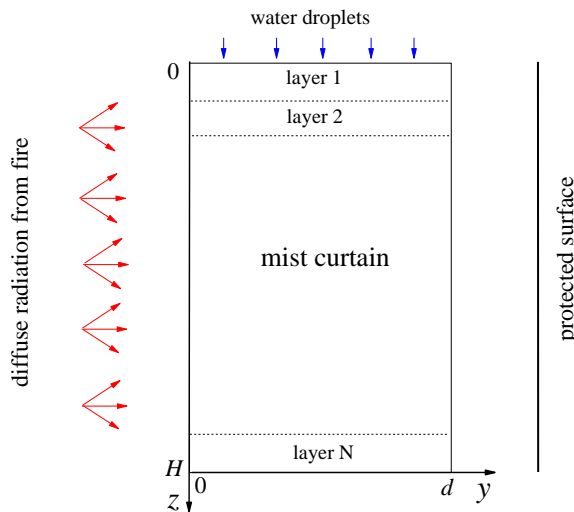


Fig. 7. Scheme of the problem for diffuse irradiation of water mist curtain.

The main but obvious assumption of the model is that there is no radiative transfer between the neighboring horizontal layers of the mist curtain and a set of 1-D solutions is sufficient. In addition, we consider the case of a relatively cold protected wall/surface and neglect possible reflection of radiation from the wall. With the use of transport approximation, the 1-D radiative transfer equation (RTE) across the mist layer can be written as follows [19]:

$$\mu \frac{\partial I_\lambda}{\partial y} + \beta_\lambda^{\text{tr}} I_\lambda = \frac{\sigma_\lambda^{\text{tr}}}{2} \int_{-1}^1 I_\lambda(y, \mu) d\mu \quad \mu = \cos\theta \quad 0 < y < d \quad (8)$$

where $I_\lambda(y, \mu)$ is the spectral radiation intensity at point y in direction μ (after the integration over the azimuth angle), $\beta_\lambda^{\text{tr}} = \alpha_\lambda + \sigma_\lambda^{\text{tr}}$ is the transport extinction coefficient. The boundary conditions at two sides of the mist layer are written as follows:

$$I_\lambda(0, \mu) = 2\pi\varepsilon_f I_b(T_f) \quad I_\lambda(d, -\mu) = 0 \quad \mu > 0 \quad (9)$$

where I_b is the Planck function. The first of boundary conditions (9) at the irradiated side of the mist curtain ($y=0$) denotes that we use the simplest assumption of an optically gray fire radiation in the model problem. In other words, the external spectral radiative flux is assumed to be directly proportional to the blackbody radiation at temperature T_f . The coefficient ε_f is the conventional constant hemispherical emissivity of the flame. It means that integral radiative flux from unit surface area of the flame is expressed as follows:

$$q_f = \varepsilon_f \int_0^{\infty} \pi I_b(T_f) d\lambda = \varepsilon_f \sigma_0 T_f^4 \quad (10)$$

where σ_0 is the Stefan–Boltzmann constant. This approach is often used in engineering calculations of fire radiation [39]. The second of boundary conditions (9) at the shadow side of the mist curtain corresponds to the assumption of a negligible irradiation of this side from the backward hemisphere by possible reflected radiation or other sources of infrared radiation.

The real mists contain particles of different size in every small volume of the medium. Strictly speaking, the calculations of spectral optical properties of the mist should take into account the local size distribution of particles. According to [10], the monodisperse approximation when all the particles are assumed to have the same Sauter radius, a_{32} , is used in the present study. In this case, the following equations are true for the absorption coefficient, α_λ , and transport scattering coefficient, σ_λ^{tr} [19]:

$$\alpha_\lambda = 0.75 \frac{f_v}{a_{32}} Q_a \quad \sigma_\lambda^{tr} = 0.75 \frac{f_v}{a_{32}} Q_s^{tr} \quad (11)$$

where f_v is the local volume fraction of particles.

It should be noted that the model presented in the current study is based on the widely used hypothesis of independent scattering [40, 41]. It means that each droplet is assumed to absorb and scatter the radiation in exactly the same manner as if other droplets did not exist. In addition, there is no systematic phase relation between partial waves scattered by individual droplets during the observation time interval, so that the intensities of the partial waves can be added without regard to phase. In other words, each particle is in the far-field zones of all other particles, and scattering by individual particles is incoherent. There is no doubt that effects of dependent scattering are negligible in the problem under consideration. At the same time, it is worth to mention that dependent scattering of microwave radiation by water droplets in cumulus clouds is really important [42].

The diffuse irradiation of the mist curtain makes the problem much simpler than that of shielding of solar radiation by water mist considered in paper [43] because there is no need for a separate consideration of directed and diffuse radiation. As a result, the two-flux method can

be employed immediately (not only to the diffuse component of the radiation field). According to the two-flux approximation the radiation intensity is presented as a combination of two angular independent components in backward and forward hemispheres:

$$I_\lambda(y, \mu) = 2\pi I_b(T_f) \cdot \begin{cases} J_\lambda^-(y), & \mu < 0 \\ J_\lambda^+(y), & \mu > 0 \end{cases} \quad (12)$$

After integration of the RTE separately over two hemispheres, one can obtain the following boundary-value problem for normalized irradiation function $G_\lambda = J_\lambda^- + J_\lambda^+$ [19]:

$$-\frac{d}{dy} \left(D_\lambda^{\text{rad}} \frac{dG_\lambda}{dy} \right) + \alpha_\lambda G_\lambda = 0 \quad D_\lambda^{\text{rad}} = 1/(4\beta_\lambda^{\text{tr}}) \quad (13a)$$

$$y=0, \quad D_\lambda^{\text{rad}} \frac{dG_\lambda}{dy} = \gamma(G_\lambda - 2)/2 \quad y=d, \quad D_\lambda^{\text{rad}} \frac{dG_\lambda}{dy} = -G_\lambda/2 \quad (13b)$$

where D_λ^{rad} is the radiation diffusion coefficient and $\gamma = \varepsilon_f/(2 - \varepsilon_f)$. The problem (13a)–(13b) at arbitrary profiles of $\alpha_\lambda(y)$ and $\beta_\lambda^{\text{tr}}(y)$ can be easily solved using the second-order finite-difference approximation and the factorization method [19]. The integral radiative flux from the shadow side of the mist layer, $q(d)$, and the profile of radiation power absorbed in the mist, $W(y)$, are

$$q(d) = 2\pi \int_0^\infty \bar{q}_\lambda I_b(T_f) d\lambda \quad \bar{q}_\lambda(d) = G_\lambda(d)/2 \quad (14)$$

$$W(y) = 2\pi \int_0^\infty \bar{w}_\lambda(y) I_b(T_f) d\lambda \quad \bar{w}_\lambda(y) = \alpha_\lambda(y) G_\lambda(y) \quad (15)$$

It is interesting to note that the above radiative transfer problem is methodologically similar to that considered recently for a cloud of sublimated silicon carbide particles suggested to protect the solar probe from intense thermal radiation of the Sun [44]. However, the present problem is simpler because the emission of thermal radiation by water droplets is negligible.

4. Water evaporation model

According to the evaporation model developed in [45, 46], it is assumed that a thin layer exists on the droplet surface (Knudsen layer) in which the vapor transfer should be considered using the kinetic theory of gases, while steam is removed from the outer boundary of the Knudsen layer due to diffusion. In this case, the following relation can be derived for the mass flow rate of evaporation:

$$\dot{m} = \frac{D p_e}{a R_{\text{air}} T_e} \ln \left(\frac{1 - \psi(T_e) \varphi_e}{1 - \psi(T) \varphi_K} \right) \quad \psi(T) = \frac{p_{\text{sat}}(T)}{p_e} \frac{M_w}{M_{\text{air}}} \quad (16)$$

where D is the diffusion coefficient, p_e and T_e are the pressure and temperature of the mixture far from the droplet surface, φ_K and φ_e are the values of air humidity at the outer boundary of the Knudsen layer and far from the droplet, respectively, R_{air} is the gas constant of air, $M_w = 18$ and $M_{\text{air}} = 29$ kg/kmol are the values of molar mass of water and air, p_{sat} is the pressure of saturated water vapor. According to recommendation of the NIST WebBook for water vapor in the temperature range of interest, the Antoine equation with the parameters determined on the basis of early data reported by Stull [47] is used:

$$\lg p_{\text{sat}}(T) = 4.6543 - \frac{1435.264}{T - 64.848} \quad (17)$$

where T is measured in Kelvin and p_{sat} is obtained in bar (10^5 Pa). The strong increasing the saturation pressure with temperature calculated using Eq. (17) is illustrated in Fig. 8a.

The value of φ_K in Eq. (16) is determined by the following balance between condition of equality of diffusion and evaporation flow rates:

$$f_{\text{ev}} \frac{p_{\text{sat}}(T)}{\sqrt{2\pi R_w T}} (1 - \varphi_K) = \frac{D p_e}{a R_{\text{air}} T_e} \ln \left(\frac{1 - \psi(T) \varphi_e}{1 - \psi(T) \varphi_K} \right) \quad (18)$$

The dimensionless coefficient f_{ev} in Eq. (18) takes into account the presence of a non-condensable component in the Knudsen layer (in our case, air). The direct numerical solution to the Boltzmann kinetic equation for the problem of evaporation of water droplets [48] enabled the authors to obtain the value of $f_{\text{ev}} = 0.0024$ which is used in subsequent calculations.

The paper [48] provided the state-of-the-art on modelling evaporation of droplets. The early monograph [49] should be primarily noted, in which the works by Maxwell and Stefan have been considered in a simple and clear manner and practically useful equations have been presented. It should be recalled that the effect of non-condensable gas components in ambient medium on the water droplet evaporation is considerable. In the simplest approach, one can consider the only non-condensable gas and solve the system of two Boltzmann kinetic equations as it was done in [48]. A comparison with the experimental data of [50] for evaporation of water droplets in ambient air confirmed good quality of this approach, which can be used in engineering models like that presented above.

An acceptable upper estimate of the evaporation rate can be obtained at $\varphi_e = 0$. The resulting variants of Eqs. (16) and (18) are as follows:

$$\dot{m} = - \frac{D p_e}{a R_{\text{air}} T_e} \ln(1 - \psi(T) \varphi_K) \quad \psi(T) = \frac{p_{\text{sat}}(T)}{p_e} \frac{M_w}{M_{\text{air}}} \quad (19)$$

$$f_{\text{ev}} \frac{p_{\text{sat}}(T)}{\sqrt{2\pi R_w T}} (1 - \varphi_K) = - \frac{D p_e}{a R_{\text{air}} T_e} \ln(1 - \psi(T) \varphi_K) \quad (20)$$

The results of numerical solution for Eq. (20) at $T_e = 300$ K are presented in Fig. 8b. The values of $D = 3 \cdot 10^{-5}$ m²/s, $R_w = 461.7$ J/(kg K), $R_{\text{air}} = 286.5$ J/(kg K), $p_e = 0.1$ MPa, $T_e = T_0 = 300$ K, are used in the calculations. The obtained value of φ_K increases monotonically with the droplet radius from $\varphi_K \ll 1$ for very small water droplets to $\varphi_K \approx 0.5$ for droplets of radius $a = 100$ μm. It is interesting that the temperature dependence of φ_K appears to be insignificant and can be even ignored in approximate calculations with the use of $\varphi_K(T_{\text{sat}})$ ($T_{\text{sat}} = 373$ K is the saturation temperature) instead of $\varphi_K(T)$. This will lead to a small overestimating of the current evaporation rate. At the same time, the effect of radius of water droplets on air parameters at the outer boundary of the Knudsen layer should be taken into account.

The above model of evaporation is more realistic than a simplified approach used in [10] because it takes into account the evaporation of heated water droplets at temperatures much less than the saturation temperature. As a result, one can obtain sufficiently accurate results for current size of water droplets and hence for the radiative flux transmitted by the water mist curtain.

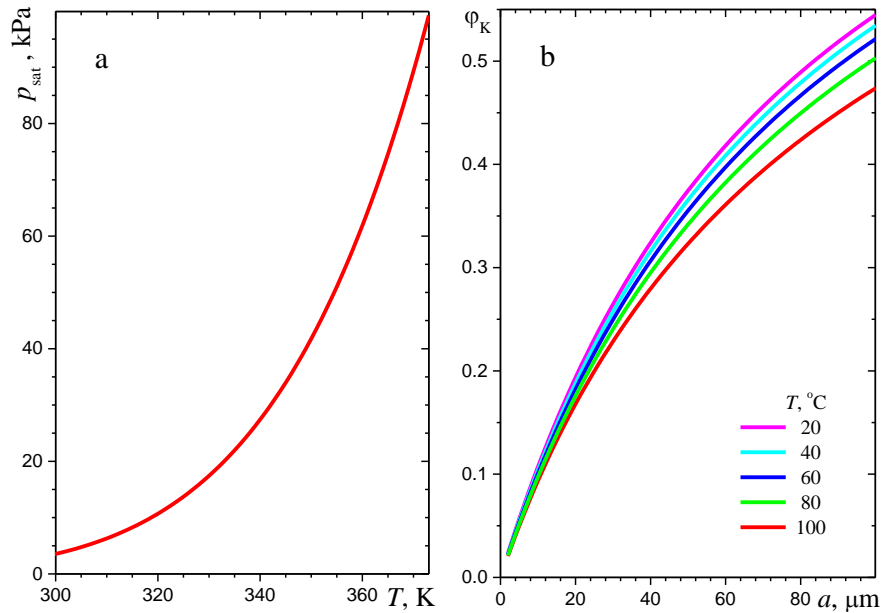


Fig. 8. Parameters of evaporation model: a – saturation pressure of water vapor, b – air humidity at the Knudsen layer boundary.

5. Initial stage of motion, heating, and evaporation of water droplets

It is interesting to consider the initial stage of motion, heating, and evaporation of droplets in a water mist curtain in more details because of both dynamic and thermal non-equilibrium

between the droplets and ambient air. The initial stage under consideration is defined as the period of a strongly variable droplet velocity and insignificant decrease in the droplet size due to evaporation. The differences in optical and thermal properties between sea water and pure water are insignificant at the beginning of the droplet evaporation. It means that the same analysis is applicable to the mist curtains of sea water as well.

It is assumed that there is no dynamic and thermal interaction between the neighbouring droplets of water, and one can consider independent equations for motion, heating, and evaporation for single spherical droplets. As usually, a good estimate for the initial stage of the droplet motion and heating can be obtained using the assumptions of both immovable and isothermal ambient gas.

According to [51–53], the following equations can be used for the droplet motion:

$$\frac{dz}{dt} = u_d \quad z(0) = 0 \quad (21a)$$

$$\frac{du_d}{dt} = g - \frac{3C_D}{8a} \frac{\rho_{\text{air}}}{\rho_w} u_d^2 \quad u_d(0) = u_{d0} \quad (21b)$$

$$C_D = 24 \left(1 + 0.15 \text{Re}_d^{0.687} \right) / \text{Re}_d \quad \text{Re}_d = 2 \rho_{\text{air}} u_d a / \eta \quad (21c)$$

where the subscripts “air”, “d” and “w” refer to the gaseous medium, droplet and water, u is the downward velocity, a is the droplet radius, C_D is the drag coefficient, g is the acceleration of gravity, η is the dynamic viscosity of air, Re is the Reynolds number.

The energy equation should take into account the external radiative heating, the convective heat transfer, and the heat loss due to the droplet evaporation:

$$\rho_w c_w \frac{dT_d}{dt} = \frac{W}{f_v} - 3 \frac{\dot{m} L_{\text{ev}}}{a} - \frac{1.5 \text{Nu} k}{a^2} (T_d - T_e) \quad T_d(0) = T_0 \quad (22a)$$

$$\text{Nu} = 2 + 0.6 \text{Re}_d^{1/2} \text{Pr}^{1/3} \quad \text{Pr} = \eta c_{\text{air}} / k \quad (22b)$$

where \dot{m} is the mass flow rate of evaporation, L_{ev} is the latent heat of evaporation, T_e is the temperature of air far from the droplet, k is the thermal conductivity of air. For simplicity, we assume that profile of the absorbed radiative power, $W(y)$, calculated at $T_f = 1500\text{K}$ and $\varepsilon_f = 0.9$, is the same as that in the initial cross section of the mist curtain. Of course, the horizontal coordinate y is just a parameter of the problem. The calculated profile of $W(y)$ for the mist curtain at $a_0 = 100 \mu\text{m}$, $f_{v,0} = 10^{-4}$, $d = 1\text{m}$ (subscript “0” refer to the initial cross section of the mist curtain) is presented in Fig. 9. The radiation power absorbed in the mist decreases from 230kW/m^3 at the irradiated side to 66kW/m^3 at the shadow side of the curtain. This leads to a significant variation of thermal conditions across the mist curtain.

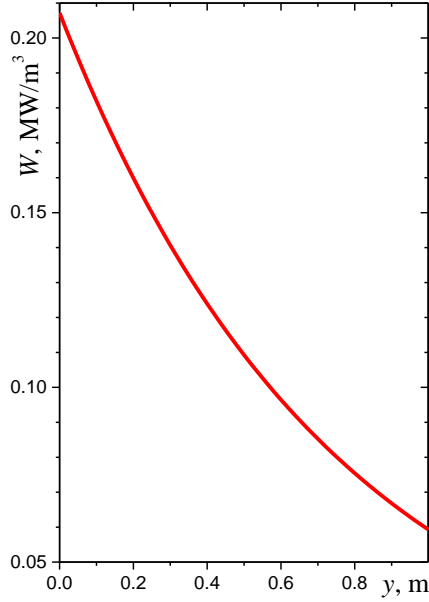


Fig. 9. Profile of the absorbed radiation power in the initial cross section of a mist curtain.

The decrease in the droplet radius due to evaporation is a solution to the initial-value problem:

$$\rho_w \frac{da}{dt} = -\dot{m} \quad a(0) = a_0 \quad (23)$$

Obviously, the local volume fraction of water droplets can be calculated as follows:

$$f_v = f_{v0} \frac{u_{d0}}{u_d} \left(\frac{a}{a_0} \right)^3 \quad (24)$$

The following values of physical parameters are used in the calculations: $u_{d,0} = 3 \text{ m/s}$, $\rho_w = 10^3 \text{ kg/m}^3$, $c_w = 4.18 \text{ kJ/(kg K)}$, $\rho_{\text{air}} = 1 \text{ kg/m}^3$, $c_{\text{air}} = 1 \text{ kJ/(kg K)}$, $\eta = 1.85 \cdot 10^{-5} \text{ Pa s}$, $k = 0.026 \text{ W/(m K)}$ and $L_{ev} = 2.26 \text{ MJ/kg}$. The large value of initial radius of water droplets ($a_0 = 100 \mu\text{m}$) was chosen to obtain the maximum estimate of the length of the region of dynamic and thermal non-equilibrium of water droplets.

Some results of calculations are presented in Fig. 10. One can see that the relaxation distance is about $z_{\text{rel}} = 0.3 \text{ m}$ for both velocity and temperature of droplets in the mist curtain. It is interesting that radiative heating of water droplets is not large due to heat losses for their evaporation. The maximum temperature of droplets is about 41°C at $z \approx 0.15 \text{ m}$ even at the irradiated side of the mist curtain. One can see in Fig. 10c that condition of very small decrease in droplet size due to evaporation at $z < z_{\text{rel}}$ is satisfied.

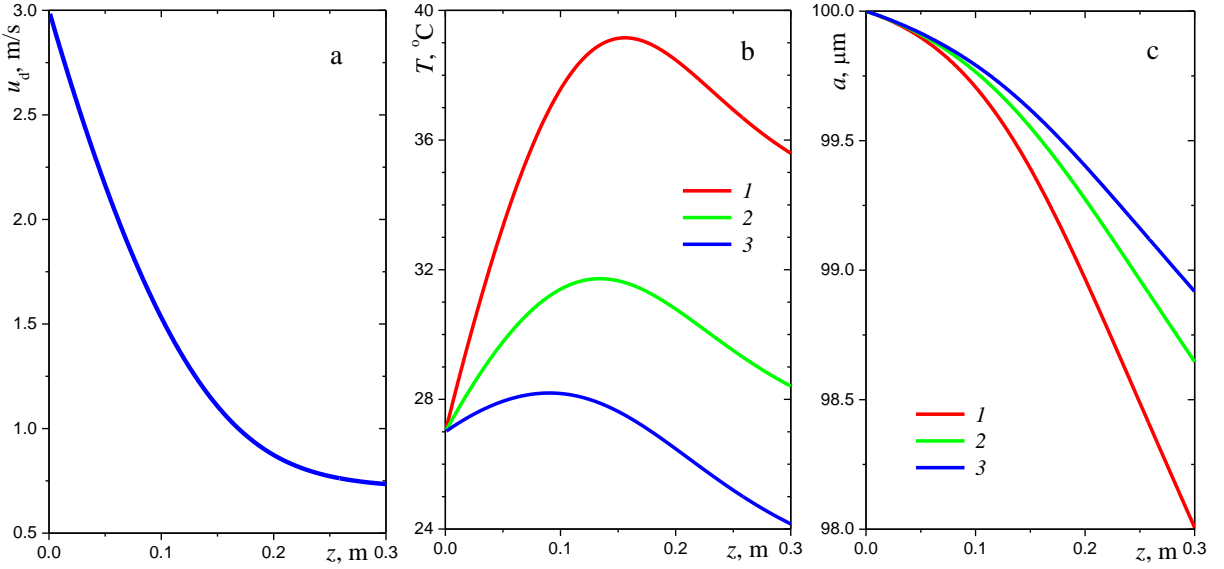


Fig. 10. Variation of (a) velocity, (b) temperature, and (c) radius of water droplets along the trajectories: 1 – $y = 0$ (irradiated side of the curtain), 2 – $y = 0.5\text{m}$, 3 – $y = 1\text{m}$.

The value of z_{rel} is much less than a typical height, H , of mist curtains. Therefore, the equilibrium approach recommended in [10] can be used in the regular computational model.

6. Completing the computational model and numerical results for water mist curtains

Following the model developed in paper [10], we focus on the central part of the mist curtain excluding the flow in the upper and lower parts of the curtain. The viscous boundary layers of the flow and the corresponding thermal boundary layers at the irradiated and shadow boundaries of the curtain are not considered as well.

For simplicity, the downward velocity of the mixture of water droplets and ambient air, u , is assumed to be constant over the mist curtain, whereas the mixture temperature, T , and the droplet radius, a , are variable in both the vertical direction and also across the curtain. It is assumed that there is no convective heat transfer between single droplets and ambient air of the same temperature and, more generally, there is no convective heat transfer across the mist curtain at all.

The mathematical problem statement for the steady-state heat transfer problem for the case of pure water is as follows:

$$(f_v \rho_w c_w + (1-f_v) \rho_{\text{air}} c_{\text{air}}) u \frac{\partial T}{\partial z} = W - 3 f_v \dot{m} L_{\text{ev}} / a \quad T(y,0) = T_0 \quad (25)$$

$$\rho_w u \frac{\partial a}{\partial z} = -\dot{m} \quad a(y,0) = a_0 \quad (26)$$

$$f_v = f_{v0} \cdot (a/a_0)^3 \quad (27)$$

The left side of energy equation (25) contains the rate of the local heat content variation for the isothermal mixture of water droplets and ambient air (per unit volume of the medium). The two terms in the right-hand side of Eq. (25) are responsible for the thermal radiation power absorbed by the droplets and the rate of heat consumption for droplet evaporation.

The absorbed radiation power, $W(y, z)$, is a function of two coordinates: the horizontal coordinate y measured from the irradiated side of the curtain and the vertical (downward) coordinate z measured from the initial cross section of the conventional equilibrium mist curtain. The above discussed spectral properties of water droplets and the model for radiative transfer in the mist curtain are used to calculate the absorbed radiation power. It should be emphasized that the coupled equations (25) and (26) are one-dimensional ones because the value of y is just a parameter of the problem. Of course, the equations of the kinetic evaporation model suggested in section 4 of the paper should be used to complete the problem statement.

It should be noted that the problem solutions at different constant values of velocity are similar to each other. Therefore, we consider the only value of $u = 2 \text{ m/s}$ in subsequent calculations. The results for another constant value of u can be easily obtained by a linear deformation of the calculated fields of all the parameters along the axis z . Strictly speaking, the realistic value of u can be estimated using the law of conservation of momentum for the supplied droplets and initially resting air. It is obvious that the value of the equilibrium velocity is determined only by the flow rate of supplied water. As before, the volume fraction of water droplets in the initial cross section of the mist curtain is assumed constant and equal to $f_{v0} = 10^{-4}$.

The results of calculations for pure water curtain of height $H = 8 \text{ m}$ are presented in Figs. 11 and 12. It is interesting that temperature of water droplets at the irradiated side of the curtain reaches the maximum value of 67°C at a distance of about 1.5 m from the initial cross section and then decreases downward. As to the monotonic decrease in droplet size due to evaporation (Fig. 11b), it seems obvious. Note that the radiative transfer across the mist curtain was systematically recalculated while solving the coupled equations. The points plotted on the curves in Fig. 12a correspond to the repeating radiative transfer calculations (one can see 17 points uniformly distributed with the interval of $\Delta z = 0.5 \text{ m}$). The additional calculations with the interval of $\Delta z = 0.25 \text{ m}$ between the radiative transfer calculations confirmed good accuracy of the results presented. We used 40, 80, and even 200 intervals along the coordinate y in the finite-difference solution of the boundary-value problem in every cross section to be sure that the radiative fluxes at both the irradiated and shadow sides of the curtain and also the profile of

the absorbed radiation power are calculated correctly. The resulting choice was 80 intervals. It appears to be sufficient for rather accurate and not too time-consuming calculations.

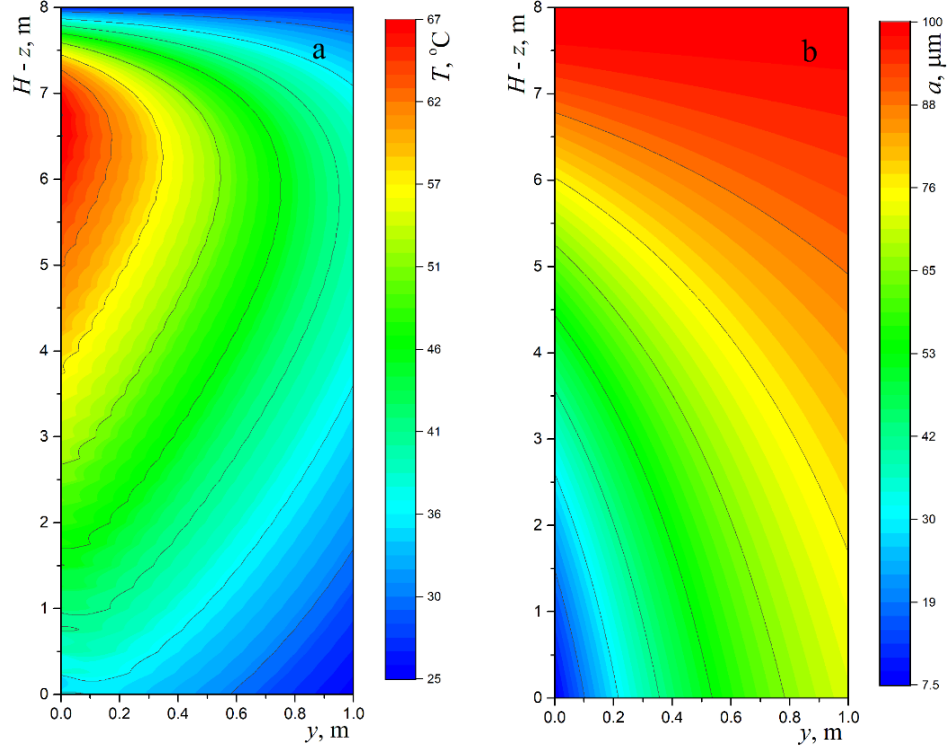


Fig. 11. The fields of (a) temperature and (b) radius of pure water droplets.

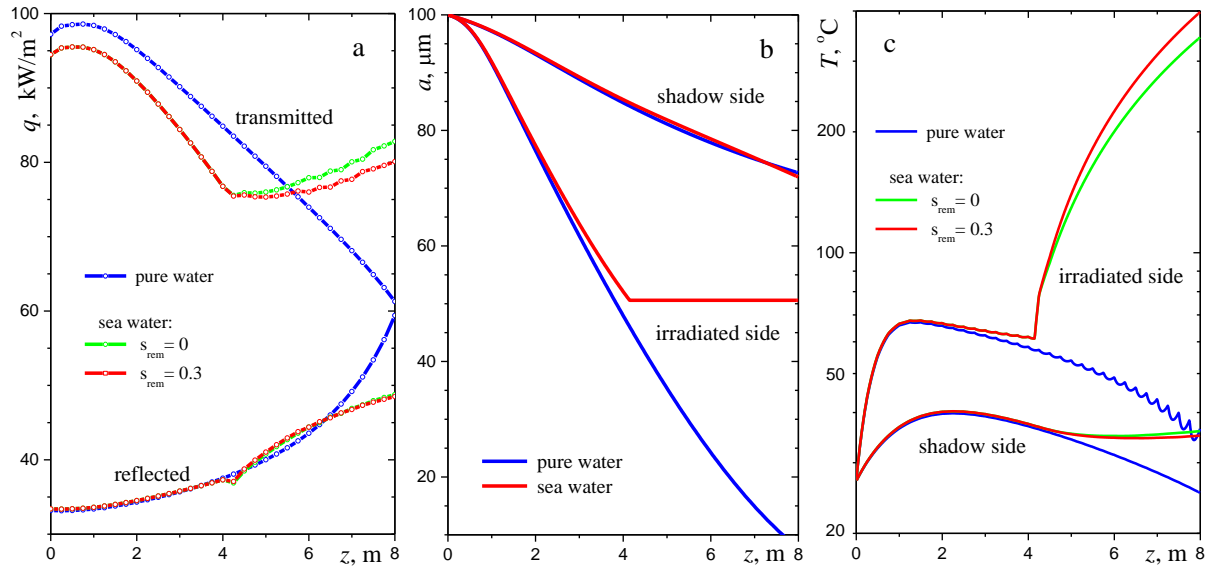


Fig. 12. Comparison of mist curtains of pure water and sea water: a – profiles of reflected and transmitted radiative flux, b – variation of particle radius along the trajectory, c – variation of curtain temperature in downward direction.

The problem statement for sea water mist curtain is more complicated than that for pure water. At the first stage of the process, one should take into account the specific properties of

sea water and their variation during the evaporation because of increased salinity of water. The current salinity of water is calculated as follows:

$$s = s_0 \frac{\rho}{\rho_w} \left(\frac{a_0}{a} \right)^3 \quad \rho = (1-s)\rho_w + s\rho_{salt} \quad (28)$$

The difference in densities of pure water and sea salt ($\rho_{salt} = 2200 \text{ kg/m}^3$) is significant and cannot be ignored. Obviously, the final expression for salinity of a sea water droplet can be written as:

$$s = \frac{s_0}{\bar{a}^3 - s_0(\bar{\rho}-1)} \quad \bar{a} = \frac{a}{a_0} \quad \bar{\rho} = \frac{\rho_{salt}}{\rho_w} \quad (29)$$

Calculations at $a_0 = 100 \mu\text{m}$ show that salinity increases slowly up to $s = 15\%$ at $a = 65 \mu\text{m}$, whereas the further decrease in droplet radius leads to a faster increase in the droplet salinity up to the maximum value. It means, that optical properties of evaporated sea water droplets on most of their trajectories until the beginning of the droplet solidification are expected to be almost the same as the optical properties of droplets of pure water. In other words, the suggested approximations for the optical properties of concentrated sea water are sufficiently accurate to be used in the problem under consideration.

The dependences of both density and heat capacity of the droplet substance with the increase in water salinity during evaporation should be taken into account in the modified Eqs. (25–26):

$$(f_v \rho_d c_d + (1-f_v) \rho_{air} c_{air}) u \frac{\partial T}{\partial z} = W - 3 f_v \dot{m} L_{ev} / a \quad T(y,0) = T_0 \quad (30)$$

$$\rho_d u \frac{\partial a}{\partial z} = -\dot{m} \quad a(y,0) = a_0 \quad (31)$$

where

$$\rho_d = (1-s)\rho_w + s\rho_{salt} \quad c_d = (1-s)c_w + sc_{salt} \quad (32)$$

The constant value of $c_{salt} = 880 \text{ J/(kg K)}$ is used in the calculations.

At the second stage of the process, the solid particles of sea salt contribute to attenuation of thermal radiation coming from a fire. The spectral optical properties of salt particles discussed in section 2.3 of the paper were used in the radiative transfer calculations to determine the absorbed radiation power. The main computational results for both sea water and pure water mist curtains are presented in Fig. 12. This figure is very instructive and enables us to draw the following conclusions:

1. The transmitted radiative flux for pure water curtain is not a monotonic function of coordinate z but decreases considerably in the lower part of the mist curtain. This is explained by a relatively strong scattering of radiation by partially evaporated water

droplets in the Mie scattering region. The latter statement is quite clear from the significant monotonic increase in reflected radiative flux with the downward coordinate (lower curve in Fig. 12a).

2. As it was expected, the difference in mist parameters at the irradiated and shadow sides of heated and evaporated mist curtain is significant, especially in current size of water droplets (Fig. 12b). In all cases, the temperature of water droplets is much less than the saturation temperature. The maximum temperature of droplets is reached in the upper part of the mist curtain and then decreases (Fig. 12c).
3. There is an intermediate stage of the process when the droplets positioned at the irradiated side of the mist curtain begin to solidify whereas the droplets positioned at the same cross section of the curtain but closer to its shadow side are completely liquid.
4. In the case of sea water curtain, the height of the evaporation region is approximately equal to a half of the total height of the mist curtain. In the evaporation region, all the mist parameters are almost the same for pure water and sea water.
5. The effect of small crystals of salt (generated by destruction of solidified saline droplets) on transmitted radiative flux in the lower part of sea-water mist curtain is very small (see Fig. 12a). The large hollow thin-walled particles of sea salt (the constant size of these particles is shown in Fig. 12b) determine the radiation shielding, which is comparable with that for the ordinary pure-water mist. A contribution of small salt particles generated in the case of possible remaining salinity of water removed from the particle is very small and can be neglected.
6. The temperature of hollow salt particles at the irradiated side of sea-water mist curtain increases strongly along their trajectories and reaches about 300 °C at the conditions of the case problem (Fig. 12c). This temperature is still too low as compared with the flame temperature to affect the heat balance, but is of interest for possible infrared diagnostics of the lower part of sea water mist curtain.

The most important practical result based on the above computational analysis is that the radiation shielding quality of a sea-water mist curtain is approximately the same as that predicted in the case of pure water.

7. Conclusions

A modified theoretical model for attenuation of fire radiation by water mist containing droplets of pure or sea water was developed. The new approach takes into account the kinetics of evaporation and also the effect of solidification of evaporated sea-salt droplets. All the calculations are based on spectral optical properties of various droplets and particles and

numerical solution for combined heat transfer in the protective curtain. The computational data illustrate the main special features of the problem and enable one to estimate the effects of problem parameters on quality of fire protection.

In the case of sea-water mist curtain, the lower part of the curtain contains thin-walled hollow particles of sea salt. These solid particles continue to attenuate the fire radiation. As a result, the radiation shielding quality of a sea-water mist curtain is approximately the same as that predicted in the case of pure water.

Of course, a simple model of the flame radiation used in the present study should be modified taking into account both the partial re-absorption of radiation in the spectral absorption bands of gases and the variation of the flame radiation power along the flame axis. After these modifications, the computational model developed is expected to be a useful tool for subsequent analysis of various engineering solutions in fire protection using water mist curtains.

Conflict of interests

None declared.

Acknowledgements

The authors gratefully acknowledge The Leverhulme Trust (project VP2-2018-010) for the financial support of this work.

References

- [1] J.-F. Sacadura, Radiative heat transfer in fire safety science, *J. Quant. Spectr. Radiat. Transf.* 93 (1-3) (2005) 5–24. <https://doi.org/10.1016/j.jqsrt.2004.08.011>
- [2] A. Collin, P. Boulet, D. Lacroix, and G. Jeandel, On radiative transfer in water spray curtains using the discrete ordinates method, *J. Quant. Spectr. Radiat. Transf.* 92 (1) (2005) 85–110. <https://doi.org/10.1016/j.jqsrt.2004.07.014>
- [3] J.-M. Buchlin, Thermal shielding by water spray curtain, *J. Loss Prevent. Proc. Indust.* 18 (4-6) (2005) 423–432. <https://doi.org/10.1016/j.jlp.2005.06.039>
- [4] P. Boulet, A. Collin, and G. Parent, Heat transfer through a water spray curtain under the effect of a strong radiative source, *Fire Safety J.* 41 (1) (2006) 15–30. <https://doi.org/10.1016/j.firesaf.2005.07.007>
- [5] S. Hostikka and K. McGrattan, Numerical modeling of radiative heat transfer in water sprays, *Fire Safety J.* 41 (1) (2006) 76–86. <https://doi.org/10.1016/j.firesaf.2005.09.003>

- [6] A. Collin, P. Boulet, G. Parent, and D. Lacroix, Numerical simulation of water spray – Radiation attenuation related to spray dynamics, *Int. J. Thermal Sci.* 46 (9) (2007) 856–868. <https://doi.org/10.1016/j.ijthermalsci.2006.11.005>
- [7] A. Collin, P. Boulet, G. Parent, M.P. Vetrano, and J.M. Buchlin, Dynamics and thermal behavior of water sprays, *Int. J. Thermal Sci.* 47 (4) (2008) 399–407. <https://doi.org/10.1016/j.ijthermalsci.2007.04.010>
- [8] W.Y. Cheung, Radiation blockage of water curtains, *Int. J. Eng. Perf.-Based Fire Codes* 1 (2009) 7–13.
- [9] G. Parent, R. Morlon, Z. Acem, P. Fromy, E. Blanchard, and P. Boulet, Radiative shielding effect due to different water sprays used in a real scale application, *Int. J. Thermal Sci.* 105 (2016) 174–181. <https://doi.org/10.1016/j.ijthermalsci.2016.02.008>
- [10] L.A. Dombrovsky, S. Dembele, and J.X. Wen, A simplified model for the shielding of fire thermal radiation by water mists, *Int. J. Heat Mass Transf.* 96 (2016) 199–209. <https://doi.org/10.1016/j.ijheatmasstransfer.2016.01.028>
- [11] L.A. Dombrovsky, S. Dembele, and J.X. Wen, Shielding of fire radiation with the use of multi-layered mist curtains: Preliminary estimates, *Comput. Thermal Sci.* 8 (4) (2016) 371–380. DOI: 10.1615/ComputThermalScien.2016017601
- [12] P. Joseph, E. Nichols, and V. Novozhilov, A comparative study of the effects of chemical additives on the suppression efficiency of water mist, *Fire Safety J.* 58 (2013) 221–225. <https://doi.org/10.1016/j.firesaf.2013.03.003>
- [13] L.A. Dombrovsky, Absorption of thermal radiation in large semi-transparent particles at arbitrary illumination of the polydisperse system, *Int. J. Heat Mass Transf.* 47 (25) (2004) 5511–5522. <https://doi.org/10.1016/j.ijheatmasstransfer.2004.07.001>
- [14] G.M. Hale and M.P. Querry, Optical constants of water in the 200nm to 200 μ m wavelength region, *Appl. Optics* 12 (3) (1973) 555–563. <https://doi.org/10.1364/AO.12.000555>
- [15] L.W. Pinkley and D. Williams, Optical properties of sea water in the infrared, *J. Opt. Soc. Am.* 66 (6) (1976) 554–558. <https://doi.org/10.1364/JOSA.66.000554>
- [16] F.J. Mullero, R.F Daniel, G.W. Wright, and T.J. McDougall, The composition of standard sea water and the definition of the reference-composition salinity scale, *Deep Sea Research. Part I: Oceanographic research papers* 55 (1) (2008) 50–72. <https://doi.org/10.1016/j.dsr.2007.10.001>

- [17] X. Li, L. Liu, J. Zhao, and J. Tan, Optical properties of sodium chloride solution within the spectral range from 300 to 2500 nm at room temperature, *Appl. Spectrosc.* 69 (5) (2015) 635–640. <https://doi.org/10.1366%2F14-07769R>
- [18] W.F. Godoy and P.E. DesJardin, Efficient transmission calculation for polydisperse water sprays using spectral scaling, *J. Quant. Spectr. Radiat. Transf.* 108 (3) (2007) 440–453. <https://doi.org/10.1016/j.jqsrt.2007.05.005>
- [19] L.A. Dombrovsky and D. Baillis, *Thermal Radiation in Disperse Systems: An Engineering Approach*, Begell House, New York, 2010. ISBN: 978-1-567000-268-3
- [20] A.A. Kokhanovsky and E.P. Zege, Local optical parameters of spherical polydispersions: simple approximations, *Appl. Optics* 34 (24) (1995) 5513–5519. <https://doi.org/10.1364/AO.34.005513>
- [21] L.A. Dombrovsky, A.A. Kokhanovsky, and J.H. Randrianalisoa, On snowpack heating by solar radiation: A computational model, *J. Quant. Spectr. Radiat. Transf.* 227 (2019) 72–85. <https://doi.org/10.1016/j.jqsrt.2019.02.004>
- [22] L.A. Dombrovsky, Spectral model of absorption and scattering of thermal radiation by droplets of diesel fuel, *High Temperature* 40 (2) (2002) 242–248. <https://doi.org/10.1023/A:1015207307857>
- [23] F.E. Volz, Infrared refractive index of atmospheric aerosol substances, *Appl. Optics* 11 (4) (1972) 755–759. <https://doi.org/10.1364/AO.11.000755>
- [24] E.P. Shettle and R.W. Fenn, Models for the aerosols of the lower atmosphere and the effects of humidity variations on their optical properties, AFGL-TR-79-0214, 1979.
- [25] R. Irshad, R.G. Grainger, D.M. Peters, R.A. McPheat, K.M. Smith, and G. Thomas, Laboratory measurements of the optical properties of sea salt aerosol, *Atmos. Chem. Phys.* 9 (2009) 221–230. <https://doi.org/10.5194/acp-9-221-2009>
- [26] D.J. Segelstein, The complex refractive index of water, Master's thesis, University of Missouri, Kansas City, 1981. <http://hdl.handle.net/10355/11599>
- [27] H. Langer and H. Offermann, On the solubility of sodium chloride in water, *J. Cryst. Growth* 60 (2) (1982) 389–392. [https://doi.org/10.1016/0022-0248\(82\)90116-6](https://doi.org/10.1016/0022-0248(82)90116-6)
- [28] P. Bharmoria, H. Gupta, V.P. Mohandas, P.K. Ghosh, and A. Kumar, Temperature invariance of NaCl solubility in water: inferences from salt-water cluster behavior of NaCl, KCl, and NH₄Cl, *J. Phys. Chem. B* 116 (38) (2012) 11712–11719. <https://doi.org/10.1021/jp307261g>
- [29] R.G. Cheng, D.C. Blanshard, and R.J. Cipriano, The formation of hollow sea-salt particles from the evaporation of drops of sea water, *Atmos. Res.* 22 (1988) 15–25. [https://doi.org/10.1016/0169-8095\(88\)90009-9](https://doi.org/10.1016/0169-8095(88)90009-9)

- [30] R. Vehring, W.R. Foss, and D. Lechuga-Ballesteros, Particle formation in spray drying, *Aerosol Sci.* 38 (2007) 728–746. <https://doi.org/10.1016/j.jaerosci.2007.04.005>
- [31] D. Fairhurst, Droplets of ionic solutions, in the book “Droplet Wetting and Evaporation. From Pure to complex Fluids”, edited by David Brutin, Academic Press, New York, 2015; Chapter 20, 295–313. <https://doi.org/10.1016/B978-0-12-800722-8.00020-5>
- [32] D.H. Charleworth and W.R. Marshall Jr., Evaporation from drops containing dissolved solids, *AIChE J.* 6 (1) (1960) 9–23. <https://doi.org/10.1002/aic.690060104>
- [33] L.A. Dombrovsky, A model for solid bubbles formation in melt-coolant interaction, *Int. J. Heat Mass Transf.* 52 (5-6) (2009) 1085–1093.
<https://doi.org/10.1016/j.ijheatmasstransfer.2008.09.024>
- [34] K. Chamaillard, S.G. Jennings, C. Kleefeld, D. Ceburnis, and U.I. Yoon, Light backscattering and scattering by nonspherical sea-salt aerosols, *J. Quant. Spectr. Radiat. Transf.* 79-80 (2003) 577–597. [https://doi.org/10.1016/S0022-4073\(02\)00309-6](https://doi.org/10.1016/S0022-4073(02)00309-6)
- [35] L.A. Dombrovsky, Approximate model for break-up of solidifying melt particles due to thermal stresses in surface crust layer, *Int. J. Heat Mass Transf.* 52 (3-4) (2009) 582–587.
<https://doi.org/10.1016/j.ijheatmasstransfer.2008.07.025>
- [36] L.A. Dombrovsky, Steam explosion in nuclear reactors: Droplets of molten steel vs core melt droplets, *Int. J. Heat Mass Transf.* 107 (2017) 432–438.
<https://doi.org/10.1016/j.ijheatmasstransfer.2016.11.064>
- [37] L.A. Dombrovsky, Scattering of radiation and simple approaches to radiative transfer in thermal engineering and bio-medical applications, Chapter 2 in the book “Springer Series in Light Scattering”, ed. by A. Kokhanovsky, Springer, 2019, v. 4, pp. 71–127.
https://doi.org/10.1007/978-3-030-20587-4_2
- [38] L.A. Dombrovsky, J.H. Randrianalisoa, W. Lipiński, and V. Timchenko, Simplified approaches to radiative transfer simulations in laser induced hyperthermia of superficial tumors, *Comput. Therm. Sci.* 5 (6) (2013) 521–530. DOI: 10.1615/ComputThermalScien.2013008157
- [39] J.L. de Ris, P.K. Wu, and G. Hesketh, Radiation fire modeling, *Proc. Combust. Inst.* 28 (2000) 2751–2759. [https://doi.org/10.1016/S0082-0784\(00\)80696-7](https://doi.org/10.1016/S0082-0784(00)80696-7)
- [40] M.I. Mishchenko, Electromagnetic Scattering by Particles and Particle Groups: An Introduction, Cambridge University Press, Cambridge (UK), 2014. ISBN 978-0-521-51992-2
- [41] M.I. Mishchenko, “Independent” and “dependent” scattering by particles in a multi-particle group, *OSA Continuum* 1 (1) (2018) 243–260. <https://doi.org/10.1364/OSAC.1.000243>
- [42] L.A. Dombrovsky and L.I. Zaichik, An effect of turbulent clustering on scattering of microwave radiation by small particles in the atmosphere, *J. Quant. Spectr. Radiat. Transf.* 111 (1) (2010) 234–242. <https://doi.org/10.1016/j.jqsrt.2009.09.003>

- [43] L.A. Dombrovsky, V.P. Solovjov, and B.W. Webb, Attenuation of solar radiation by water mist and sprays from the ultraviolet to the infrared range, *J. Quant. Spectr. Radiat. Transf.* 112 (7) (2011) 1182–1190. <https://doi.org/10.1016/j.jqsrt.2010.08.018>
- [44] L.A. Dombrovsky, D.L. Reviznikov, A.P. Kryukov, and V.Yu. Levashov, Self-generated clouds of micron-sized particles as a promising way of a solar probe shielding from intense thermal radiation of the Sun, *J. Quant. Spectr. Radiat. Transf.* 200 (2017) 234–243. <https://doi.org/10.1016/j.jqsrt.2017.06.025>
- [45] A.P. Kryukov, V.Yu. Levashov, and S.S. Sazhin, Evaporation of diesel fuel droplets: Kinetic versus hydrodynamic models, *Int. J. Heat Mass Transf.* 47 (12-13) (2004) 2541–2549. <https://doi.org/10.1016/j.ijheatmasstransfer.2004.01.004>
- [46] V.Yu. Levashov and A.P. Kryukov, Numerical simulation of water droplet evaporation into vapor–gas medium, *Colloid J.* 79 (5) (2017) 647–653. <https://doi.org/10.1134/S1061933X1705009X>
- [47] D.R. Stull, Vapor pressure of pure substances. Organic and inorganic compounds, *Industr. Eng. Chem.* 39 (4) (1947) 517–550. <https://doi.org/10.1021/ie50448a022>
- [48] V.Yu. Levashov, A.P. Kryukov, and I.N. Shishkova, Influence of the noncondensable component on the characteristics of temperature change and the intensity of water droplet evaporation, *Int. J. Heat Mass Transf.* 127 (2018) 115–122. <https://doi.org/10.1016/j.ijheatmasstransfer.2018.07.069>
- [49] N.A. Fuchs, *Evaporation and Droplet Growth in Gaseous Media*, Pergamon Press, New York, 1959.
- [50] V.Y. Borodulin, V.N. Letushko, M.I. Nizovtsev, and A.N. Sterlyagov, Determination of parameters of heat and mass transfer in evaporating drops, *Int. J. Heat Mass Transf.* 109 (2017) 609–618. <https://doi.org/10.1016/j.ijheatmasstransfer.2017.02.042>
- [51] J. Hua, K. Kumar, D.C. Khoo, and H. Xue, A numerical study of the interaction of water spray with fire plume, *Fire Safety J.* 37 (2002) 631–657. [https://doi.org/10.1016/S0379-7112\(02\)00026-7](https://doi.org/10.1016/S0379-7112(02)00026-7)
- [52] C.T. Crowe, J.D. Schwarzkopf, M. Sommerfeld, and Y. Tsuji, *Multiphase Flows with Droplets and Particles*, Second edition, CRC Press, New York, 2011. <https://doi.org/10.1201/b11103>
- [53] L.A. Dombrovsky, S. Dembele, and J.X. Wen, An infrared scattering by evaporating droplets at the initial stage of a pool fire suppression by water sprays, *Infrared Phys. Technol.* 91 (2018) 55–62. <https://doi.org/10.1016/j.infrared.2018.03.027>